Hume-Rothery for HEA classification and Self-Organizing Map for phases and properties prediction

M. Calvo-Dahlborg[1,*] and S.G.R. Brown[2]

[1] GPM UMR6634-CNRS, University of Rouen Normandie, Campus Madrillet, BP12 76801 Saint-Etienne-du-Rouvray cedex, France; monique.calvo-dahlborg@univ-rouen.fr

[2] College of Engineering, Swansea University Bay Campus, Fabian Way, Swansea, Neath Port Talbot, SA1 8QQ, UK; s.g.r.brown@swansea.ac.uk

*Corresponding author: monique.calvo-dahlborg@univ-rouen.fr

Abstract: The Hume-Rothery approach applied in terms of *e/a* to classify and design quasicrystals and BMG is revisited for the case of HEAs. The results were compared with other parameters used in the literature, namely VEC and delta. The Self-Organizing Map tool is used to classify the experimental results and the experimental map is used to compare the predictions of phases and properties of compositions reported in the literature. According to the Hume-Rothery approach e/a and the average radius can give a precise rule of thumb to identify the domain of stability of HEAs and to estimate the phases that may occur in the alloy: i) $e/a < 1.65$: *fcc*, ii) $1.65 < e/a < 2.05$: mixed phases including in particular *sigma*, iii) $e/a > 2.05$: *bcc*. Moreover, e/a is to be preferred to VEC to classify phases in HEAs and the simple combination of *e/a* and *r* give more accurate estimation than complex approaches based on DOS and VEC. Self-organizing maps can be used to make interpolative predictions for new compositions of HEAs with suitable phases for specific properties.

Keywords: HEA, e/a, phases, Self-organizing maps, magnetic, Hume-Rothery.

1. Introduction

The term “high entropy alloys” has been introduced in 2004 to name alloys in equimolar or near-equimolar amounts [1-2]. However, a new metallurgy was born by considering not one or two main elements with the others as minor additions but with all elements on an equal footing from the liquid state. Thus, a new name appeared, closer to the reality of this new metallurgy, “multi-principal element alloys”, MPEAs [3]. For simplicity, we will stick to the initial term “HEA” in the following.

In the last 12 years, many reports have reviewed the observed structures and microstructures as well as the potentialities of these new alloys in terms of applications of different kinds. The most cited report [4] defined HEAs, as compared to Bulk Metallic Glasses (BMGs) and intermetallics in terms of the parameter *omega*, dependent on the entropy of mixing, versus the atomic mismatch, *delta*. The existing location for HEAs was defined at *omega* $\geq$ 1.1 and *delta* $\leq$ 6.6%. This work [4] has strongly influenced the search for more HEAs.

Determining the phases stable after solidification in high entropy alloys has been an important issue since their discovery as the resulting phases influence the mechanical efficiency of the alloy and thus the potential applications. Generally *fcc* phases favour ductility and *bcc* phases favour strength. Scientific issues and challenges have been discussed including aspects of definition/terminology, phase formation, microstructure and phase stability, strengthening mechanisms, and high temperature properties, as well as the density and cost [4-10].

Several studies were aimed at finding single-phase HEAs [11-16]. In [14], it was claimed that single phase *fcc* solid solution should form if *delta* <4.27%, -7.27 kJ mol^{-1}<enthalpy of mixing <4 kJ mol^{-1} and the total valence electron (*VEC*)>8. While a single phase *bcc* solid solution should form if *delta*<4.27%, -7.27 kJ mol^{-1} <enthalpy of mixing<4 kJ mol^{-1} and *VEC*<6.87.

Less empirical methods using numerical calculations and models have been developed to identify desired or undesired phases and to classify and/or design HEAs. The CALPHAD approach has been widely used to achieve an understanding of phase stability and phase relationships [3,7,8,17-20]. However, it was concluded in [17] that none of these criteria (entropy of mixing, variations in atomic radius, electronegativity, valence or number of itinerant electrons, lattice distortion), taken alone, can reliably predict the formation of a single solid solution.

Thus, more complex methods using other characteristics and parameters other than entropy of mixing and mismatch were proposed including lattice distortion, hardness and the total (*VEC*) or reduced (*e/a*) number of valence electrons [21-29]. The comparison with BMGs is often

mentioned [4,21,24,30]. In [21], the authors claim that the two chosen parameters of the method clearly provide separate regions for *fcc* and *bcc* by displaying solid solutions, intermetallics, bulk metallic glasses and other crystal structures.

In this work, the Hume-Rothery approach applied in terms of *e/a* to classify and design quasicrystals and BMGs [31-37] is revisited for the case of HEAs. Furthermore, the present work has the aim to provide a new general tool for classification of HEAs via potentially occurring phases and a potential methodology for interpolative prediction for HEAs. Data from both as-cast and homogenized alloys have been used. New compositions, the effects of thermomechanical treatments and specific industrial applications have not yet been considered,

2. Materials and Methods

2.1 Experimental details

235 different compositions were used in this work, based on 3 to 9 elements out of the total 25 different elements constituting the whole set of alloys:

- Among them, ingots of 67 compositions were chosen for analysis using a Self-Organising Map (SOM) map approach, described below. The alloys [38-43] prepared by different techniques were investigated with a superconducting quantum interference device (SQUID) at temperatures from 5 to 400K. The average magnetic moment per atom as a function of applied magnetic field was measured at 5K and the saturation value was estimated whenever possible. The plotted values are given in Bohr Magneton for comparison. In order to determine the structure of the alloys at the atomic level three different experimental diffraction techniques were used: standard X-ray diffraction (XRD), high-energy X-ray diffraction (HEXRD) and neutron diffraction (ND) [38-43]. It is thus to be noted that the resolution of the determination of the existing phases in the alloys used in the map for the classification and prediction is very high as detailed in [41]. An arbitrary number has been attributed to each of the phases detected: 1 for *fcc*, 2 for *bcc*, 3 for *hcp*, 4 for B2, 5 for unknown, 6 for *sigma*, 7 for other phases, 10 for multiple. “Unknown” refers to phases not possible to identify and “multiple” to a very complex diffraction pattern, appearing as “forest-like”. The detailed experimental results for these alloys are reported elsewhere.

- The results of the observed phases for additional 146 compositions were taken from [10] and 22 from [28] for the prediction part.

The total, 2P, of the first two main identified phases has been chosen as one experimental value for classification purposes, e.g. 2P=6 for *bcc* and B2 or 3 for *fcc* and *bcc*. It is distinguished in the figures below between the following cases: *fcc* only, *bcc* only, *fcc* main plus one *bcc*, *bcc* main plus one *fcc*, two *fcc*, two *bcc*, one *bcc* and one B2. Moreover, when another phase is identified as a third phase, it is also specified in the symbols but it is not counted in the 2P summation. For example an alloy for which a *bcc* and a B2 have been identified as first two main phases but also an *fcc* as third phases, 2P will be equal to 6 but the value will be identified in the plot by three symbols: *fcc*, *bcc*, *bcc*+B2.
Thus, only part of the experimental data used in this work come from our own results, the rest being taken from the literature.

2.2. Self-Organising Map

The current work also uses a basic Self-Organising Map (SOM) [44-47] to classify the 67 alloys for which the magnetization at saturation (or the maximum one) had been measured. 15 different parameters were available per each alloy, as listed in table 1. SOM are commonly used to draw trends in multiple parameters characterization in various domains. Their application to the case of HEAs was to try to observe if the various 15 parameters available for the investigated alloys are aligning themselves naturally. Also, the ability of the SOM approach to be used in a predictive capacity is investigated, albeit in an interpolative prediction mode.

These 15 parameters are defined as the vector **ALLOY** and are stored in a 67 by 15 array. SOMs provide a methodology for representing such multidimensional data in a much lower dimensional format, usually in the form of a 2D map [44]. SOMs are widely described in the general literature so only a brief overview is provided here [44-47]. Initially each parameter in the vector **ALLOY** is individually scaled from 0 to 1 (e.g. all average radii are scaled between 0 and 1 etc.). A training vector is then selected. The training vector consists of a subset SUB containing n selected parameters from **ALLOY**, where **SUB⊂ALLOY**. A 20x20 grid of nodes is then set up where each node initially possesses its own uniformly distributed random values, from U(0,1), for each parameter in **SUB**. Construction of the SOM proceeds by repetition of the following 'time' steps, *t*.
1: Randomly select an alloy (1 to 67), $\mathbf{ALLOY_x}$.

2: Determine the node that most closely matches the chosen alloy, i.e. the node that minimizes the expression, $Node = \sqrt{\sum_{i=1}^{n}(\boldsymbol{SUB}_i - \boldsymbol{ALLOY}_x)^2}$. The chosen node is now defined as the **best matching unit** or **BMU**.

3: Next, the neighbourhood of the **BMU** is determined. The neighbourhood is made up of those nodes that are within a fixed distance of the **BMU**. This fixed distance decreases as more steps are performed so that **BMU** neighbourhoods become smaller as the number of iterations increases.

4: Within this neighbourhood **SUB** is adjusted to move towards $\mathbf{ALLOY_x}$ by an amount inversely proportional to the distance of the neighbourhood node from the **BMU**,

$\mathbf{SUB}^t = \mathbf{SUB}^{t-1} + \Theta(t)\ (\mathbf{ALLOY_x}\text{-}\mathbf{SUB}^{t-1})$

Where the weighting function $\Theta(t)$, the so-called learning rate, is an inverse function of the distance of the neighbourhood node from the **BMU**. $\Theta(t)$ also decreases linearly with increasing time steps, *t*.

5: The process is then repeated N times until the fixed distance defining the **BMU** neighbourhood becomes just one node.

Once this process is finished the **BMU** for each alloy is then determined and the alloys are placed on the map at their **BMU** locations. To aid the reader a flow chart of the basic SOM code is presented in figure 1.

2.3. Set-up of the classification

2.3.1. Hume-Rothery approach

As pointed out in [27] the simplicity and the generality of the Hume-Rothery rules helped to achieve the prediction of solubility in alloys [48-50]. Moreover, Hume-Rothery and his co-workers demonstrated the importance of the electron-to-atom (*e/a*) ratio in controlling the range of stability of solid solutions, intermetallic compound formation and liquidus temperatures in metals and alloys. Based on this, several authors demonstrate that the variation of properties as a function of the number of valence electrons is a useful approach to classify and design alloys [51-54]. A review on the use of *e/a* to design alloys with specific properties can be found in [51].

However, several authors noted the non-validity of Hume-Rothery rules in the case of intermetallic compounds and have thus proposed adapted rules and new *e/a* values based on Full-Potential Linearized Augmented Plane Wave (FLAPW) band calculations [55-57]. It is to be noted that due to their compositions several intermetallic phases are detected in some

HEAs. Several authors claim that the name HEA should be restricted to alloys containing simple phases such as fcc, bcc and hcp and thus corresponding to simple diffraction patterns. The present study is focused on classifying alloys as a function of the potential phases which can occur, and thus to predict new HEA compositions for potential applications needing one phase or the other or a combination of several. Other types of investigation, e.g. using ab initio electronic structure calculations, are of course not excluded after this proposed first selection test based on e/a and r. Other types of investigation could be used to refine the structure, composition and application of newly discovered alloys.

A solid solution is defined in the literature as a homogeneous crystalline structure in which one or more types of atoms or molecules may be partly substituted for the original atoms and molecules without changing the structure. In a first approximation to solid solutions all the parameters used in SOM were chosen as the sum of the parameters of the constituting elements of the alloy weighted by their respective atomic percentage in the composition. However, the approximation is not an overestimation the phases considered to exist in HEAs are *fcc*, *bcc* and *hcp,* the complex intermetallic ones being additional.

The first Hume-Rothery rule states that, if the atomic diameters of the solvent and solute differ by more than about 14-15% then the primary solid solubility will be very restricted. HEAs are multicomponent [2] and multi-principal element alloys [3] and close to equiatomic concentrations are usually considered. Thus, all elements are on equal footing in terms of solidification in this rule.

Consequently, the restrictions of the first rule do not apply to solidification and the second rule emphasizes the importance of the electron concentration (or electron per atom ratio).

2.3.2. Choice of e/a

Hume-Rothery rules state that particular alloy crystal structure types are found at specific electron *e/a* values. In the case of transition metals forming generally complex intermetallic phases, the validation of these rules has been widely discussed and band and density of states calculations as well as artificial neural networks approaches were developed in order to estimate more suitable e/a values [55-62]. Mizutani proposed new values for e/a in [56]. These values have been used in fig. 2d for comparison.

However, as detailed in [63], it is important to stress that one can express the electron concentration in two ways. One is the *VEC*, more recently referred to as the valence electron concentration, where all the electrons are counted including the *d*-electrons (and other

electrons) accommodated in the valence band. The other one is *e/a*, the number of itinerant electrons per atom. Depending on the type of material, *e/a* or *VEC* have to be considered when applying the Hume-Rothery approach.

Recently Hume-Rothery rules were applied, especially using *e/a*, for new types of alloys, namely quasicrystals to develop a classification and discover new compositions. In this case no calculations but rather empirical rule were used to predict the ternary quasi-crystal compositions from binary ones. Furthermore it was demonstrated that Quasi-Crystals (QCs) are Hume–Rothery phases [31-34].

Furthermore, as was pointed out in [63] the calculations of valence electrons for a system is sometimes not correctly estimated, with confusion between the *VEC*, the total number of valence electrons and *e/a*, and the *s* and *p* electrons. For example, in [28], a series of high-entropy equiatomic alloys have been analysed to determine the main factors that influence the formation of various solid solutions and chemical compounds. The key factor leading to the formation of phases in high-entropy equiatomic alloys is said to be the mean electron density (*e/a*) but in fact *VEC* values are used. Similarly in [64] *e/a* and *VEC* are mixed in the classification of simple structure types using Hume-Rothery rules.

In the following, the *e/a* and *VEC* values have been calculated, in the standard way, according to [63]. For example in the case of Zn, with $3d10^4s^2$ as electronic structure and 2 electrons in the outside layer, e/a=2 and VEC=12. Applying a solid solution first approximation, the e/a and VEC for the alloys have been calculated from their atomic compositions as a linear combination of the e/a and VEC of the individual constituting elements.

Accordingly, we have preferred the standard e/a data from Massalski/Hume Rothery for the calculation of e/a and VEC in the case of our study for the following reasons:

1) HEA can be firstly approximate as solid solution due to their close to equiatomic composition and to the phases usually detected, namely fcc, hcp and bcc.

2) The Hume Rothery approximation that e/a can be used to distinguish domains of existence of phases works in the case of solid solution.

3) Alloys with compositions close to HEA and containing complex intermetallic phases are not HEA as they thus do not have a simple diffraction patterns [41]. We thus have not used the e/a values from Mizutani.

Furthermore the aim of the classification/prediction presented in this study is not to find compositions with complex intermetallic phases but composition with simple phases giving simple diffraction patterns, thus true HEAs. Thorough investigations, e.g. using electronic structure calculations are considered as belonging to the second step.

2.3.3. Choice of r

For another class of materials, namely BMGs, it was shown that two criteria were necessary to discuss the stabilization mechanism of metallic glasses, *e/a* and average atomic size [35-37].

As pointed out in [48] the exact "atomic diameter" of an element is always difficult to define. The atomic distances used in Hume-Rothery approach are defined [50] as the closest distances of approach of atoms in the crystals of the elements. The radii given in [65] are probably the most useful for discussing metallic alloys as they are reported for a coordination number of 12. They were taken from the observed interatomic distances in *fcc*, *hcp* and *bcc* structures. However, this diameter cannot necessarily be transferred to the alloy because the 'radius' of an atom is affected by coordination number.

Here we considered that HEAs are not binary, but equimolar with a minimum of 3-4 elements. Thus, only the average radius according to [65], and not the mismatch was considered in the classification. However, a display of the properties versus the mismatch values, delta, is also performed below for comparison.

Applying a solid solution first approximation, the average radius for the alloys has been calculated from their atomic compositions as a linear combination of the radius of the individual constituting elements. Providing error bars for all of the calculated data (average radius, mismatch, e/a, VEC) is acknowledged as challenging referring as it does to commonly used databases of physics, such as the radius for bcc, fcc and hcp structure (Teatum, reference [65]) and the number of different electrons per atom.

3. Results

3.1. Two dimensional plots of experimental results and bibliography data

In [51, 63], the relation between phase formation and magnetism was stressed for choosing *e/a* to classify alloys. Furthermore, BMGs and HEAs are often compared [4,24]. Thus, we have chosen to investigate in detail the variation of M, the average magnetic moment per atom at 5K, and 2P, the first two detected phases, as experimental properties to be classified

as a function of *e/a* and the average radius. Figure 2, a to c, presents the variation of M for 67 compositions [38-43] as a function of standard *e/a*, *delta* and *VEC* as well as the *e/a* values proposed by Mizutani in [55-57], respectively, for the detected phases. The M values get classified into two (figure 2, b and c) or three domains (figure 2, a and d). The comparison of figure 2a and figure 2d confirms that the use of the proposed calculated values of Mizutani [55-57] for transition metals does not give better results than the simple standard ones calculated according to Massalski/Hume Rothery [63].

Lines were drawn in order try to separate domains of *fcc*, *bcc*, and mixed phases in figure 2, a to c.Two regions are apparently observed versus *delta* and *VEC* in figure 2, b and c, although there is some overlap. According to the literature [4,17], HEAs should form at *delta* < 6.6. As shown in figure 2b, the investigated alloys from [38-43] and [10, 28] are in this region. Thus, nothing can be concluded. As strongly emphasized in [10], the *delta* based classification has limited use in terms of controlling the formation of *fcc*- or *bcc*-structured HEAs because the *fcc*-type solid solution forming *delta* range largely overlaps with that of *bcc* solid solutions.

Figure 3, a and b, presents the variation of *e/a* as a function of the sum of the two main phases detected and of the average radius, respectively. The values correspond to the alloys of figure 2 as well as to other compositions from the literature [10,28]. Lines were drawn in order try to to separate domains of fcc, bcc, and mixed phases in fig. 3, a and b.

When the four parameters discussed in part 2 are combined, namely e/a, the atomic radius, the average magnetic moment per atom and the two first detected phases by diffraction, presented in fig 2a, 3a and 3b, the following domains can be identified:

i) *e/a*< 1.65: *fcc*,

ii) 1.65< *e/a* < 2.05: mixed phases including intermetallic phases, in particular *sigma*,

iii) *e/a* > 2.05: *bcc*.

Because of the controversial use of *e/a* values for transition metals (TMs) *VEC* has often been preferred to study the electron concentration effect on phase stability in HEAs and has been presented by several authors as a key parameter to classify HEAs [14,17,21,24,26]. For comparison the variation of *VEC* for the same alloys [10,28,38-43] as a function of the two main detected phases as well as the average radius are presented in figure 4, a and b.

However, if *fcc* phases in HEAs seem to stabilize preferentially at higher *VEC*, the *bcc* phases do not only occur at lower *VEC* (figures 2c and 4). The division in three domains is much clearer when using e/a (fig. 3 a and b) as when using VEC (fig. 4 a and b). However, HEA compositions can lead to the occurrence of intermetallic phases. The present classification

aims to distinguish between the fcc, the bcc and the other phases. In this paper it is considered that the use of e/a is more appropriate for this aim.

In [29], the authors claim that *VEC* is the physical parameter controlling phase stability in HEAs and that *fcc* phases should be stable for *VEC*>8 and *bcc* ones for *VEC*<6.87. In figure 4a, *bcc* phases can be found in both regions, they are not only localized in one single domain.

In [13] structure and hardness are predicted as a function of *VEC* and *delta*. The authors claim that *fcc* structure is found for 7.80 < *VEC* < 9.50 and *bcc* for 4.33 < *VEC* < 7.55. The domain for *fcc* occurrence fits with the results presented figure 4a. However, bcc structure appears in a much larger region.

More complex approaches have been developed in order to classify HEAs using several parameters, including both *delta*, *e/a* and *VEC* [14,21,24]. In order to compare with these works, the variation of *VEC* as a function of *delta* and *e/a* as a function of *VEC*, with indication of the two main phases is presented figures 5 and 6 respectively with the domains identified in [14] and [24] delimited in colour.

In [14] an empirical rule is proposed and it is claimed that *fcc* forms if *delta* <4.27 and *VEC*>8, and *bcc* if *delta* <4.27 and *VEC*<6.87. The coloured regions on figure 5 represent the two identified regions. Although the fitting is rather good for *fcc*, it completely fails for *bcc*.

In [24] using a thermodynamic approach and the application of Hume-Rothery rules the authors claim that *fcc* phases are stabilized by *VEC*>7.5 and 1.6< *e/a* < 1.8 and *bcc* at *VEC* <7.5 and 1.8<*e/a* <2.3. These regions are identified with colours in figure 6a. However, the fit is not apparent especially for the *fcc* region.

In the complex classification proposed in [21] the interatomic spacing distribution and the bulk modulus distribution are also introduced. It is claimed on a representation of *e/a* versus *VEC* that these two parameters accurately separate *fcc* and *bcc* regions, in particular for some *fcc* and *bcc* alloys. These three regions are represented in figure 6b. The regions are located where *fcc* occurs for the *fcc* domain in [21] and where *bcc* occurs for the *bcc* domain. However, in two regions out of three, additional phases have also been observed.

From the first 2D plots of figures 2 to 6, the following conclusions can be drawn:

1) The classification of the alloys in three domains by *fcc*, mixed and *bcc* with the use of *VEC* and *delta* is not very efficient. In particular the values corresponding to the alloys containing bcc phases are widely spread.

2) As expected from the literature and discussed above in part 3, properties can be organized if they are plotted as a function of *e/a* in case of magnetic properties. Moreover, two of the well identified domains correspond to the simple phases, namely *fcc*, *bcc* and *hcp*.

3) Furthermore, the domain between *e/a*=1.65 and *e/a*=2.05 define an interval where no "real" HEAs can be found, i.e. where the diffraction pattern is not simple as defined in [39, 41].

3.2. Mapping of the experimental results

In order to get a picture of several combined parameters the Self-Organising Map (SOM) approach has been used. In order to differentiate the influence of some parameters not all of them are necessarily used to construct the map. Thus, *e/a*, *VEC*, the first identified phase by diffraction, the second phase, the sum of the first two main phases (2P), the density, the atomic mass, the mismatch delta, the average radius, the hardness, the average magnetic moment per atom at 5K and 300K and the average volume per atom have been combined with one another and tested for their efficiency in reproducing the results from figures 2 and 3. See Table 1 for the list of these parameters.

Figures 7, a to f, presents the results arising from the selective choice of *e/a*, *delta*, *VEC*, *M* at 5K, the 1st detected phase, the 2nd detected phase to make up the training vector. Thus, in this case **SUB** = *e/a*, *delta*, *VEC*, *M* at 5K, the 1st detected phase, the 2nd detected phase and these six parameters alone are used to construct a single SOM. Once the SOM is constructed the resulting distribution of the individual parameters within it can be visualized.

The maps show the locations of the different alloys (labelled as M1, M2 etc.). The alloys are always at the same positions on the maps shown in figures 7 a-f. One can observe that the domains in figure 7a and 7d, corresponding respectively to *e/a* and *M* at 5k, are correlated. As in figure 2a, the lowest values in *e/a* correspond to high values of *M* (figure 7a) and low values in first and second phase, *fcc*, (figure 7, e and f). This also corresponds to middle values of *VEC* (figure 7c). As in figure 2a, the other domains of high values of *e/a* (green and red in figure 7d) correspond to the high values of *M* in figure 7a. This also corresponds to high values in *delta* (figure 7b). But no other real correlations can be observed.

Thus, figure 8, a to f, has been produced by reducing the parameters of interest from six to the two discussed in part 3.2 and 3.3 and represented in figure 3, a and b, namely *e/a* and the average radius. In this case **SUB** = *e/a* and *r*. The data for *M* at 5K and 2P, the average magnetic moment per atom and the sum of the two main detected phases by diffraction (as

shown in fig 2a and 3a) are not used to construct the map. Their distribution on the map is only visualised after the SOM has been created. Although *M* at 5K and 2P were not used to construct the map, figure 8, c and d, show their strongly correlated distribution. Figures 8a and 8c on one side and figures 8b and 8d on the other side are correlated. The highest and lowest values of *e/a* in figure 8a (red and blue) correspond to the highest values of *M* in figure 8c (green and red). The mainly *fcc* domain in figure 8d correspond to the lowest values in *e/a*, *r* and *M* in figures 8, a, b and c respectively.

For confirmation, figure 9, a to d, presents this same choice of **SUB** using the same data but with the SOM started from a different start point in the pseudorandom number sequence. As expected the alloys are not in the same place from figures 8 to figures 9 but the same correlation can be observed in figures 9a and 9c and in figures 9b and 9d. The different choice of random number to start the SOM does not affect the underlying relational organization of data in the map.

Thus, it appears, as expected from the literature and detailed in part 2.3, that the two parameters, *e/a* and *r*, are sufficient to produce a map with correlated *M* at 5K and 2P.

3.3. Predictions compared with literature

The SOM approach has been used above in a first step to describe, in a visual format, the different phases identified as indicated in [10] and [28]. It is now used in a second step to assess its ability to make interpolative predictions for new alloys.

Figure 10 is figure 2a including the predicted values of *M* at 5K from the SOM procedure from the *e/a* and *r* of the alloys investigated in [10] and [28]. Figure 11 presents the phases predicted by the SOM from the e/a and r of alloys from [10] and [28]. These values are predicted by identifying the **BMU** on the pre-calculated SOM for the new alloys and assigning the data associated with the **BMU** to the new alloy. Importantly, the SOM used to classify the new alloy is constructed without knowledge of the new alloy data. This represents an interpolative prediction. The vertical lines represent the three domains identified in Fig 2 where only the experimental data from the map (from [38-43]) were plotted. Figures 10b and 11b present figure 10a and 11a without the alloys for which only *fcc* phases were identified, namely without *fcc* and *fcc*+*fcc*. Figures 10c and 11c present figure 10a and 11a without the alloys for which only *bcc* phases were identified, namely without *bcc* and *bcc*+*bcc* and *bcc*+B2.

The variation of the predicted values for both the *M* at 5K (fig 10) of the alloys from literature [10, 28] follows the same variation as the experimental ones from [38-43] (fig. 2a). Fig 11

presents the same three domains of appearance of the phases, especially the domain where other phases than *fcc*, *bcc* and *hcp* occur.
Thus, it appears that Self-Organizing-Maps based on e/a and r can be used predictively for new compositions of HEAs alloys. The comparison between the predicted and the reported two main phases for alloys of [10,28] is well (fig 11a), especially for *fcc* phases (fig 11c). However, for *bcc* phases (fig 11c) some predicted 2P values have been set to 0 by the SOM. The observed limitations of the map are the following:

- The predicted values depend on the initial values of the map used for the SOM approach. For example, some of the alloys of the map had no defined values for 2P because they had not been analysed by diffraction. Thus, their 2P values were 0. This has thus introduced 0 as a possible value for the further prediction, especially for the *bcc* alloys (fig 11, a and b).

- Furthermore, the SOM approach cannot create an extrapolated value outside of the data used to construct the map. For example, the prediction for the *M* at 5K for the AlNiCo alloy has not resulted in a value larger than the maximum value present on the original map. This drawback must be taken into account when constructing the map. The use of alloy data containing a wide range of values to initially construct the SOM can help to reduce this drawback.

It is to be emphasized that the SOM presented in this study, i.e. based on e/a and r and to predict M at saturation and 2P, has been used to confirm new compositions which have been produced and which are now being investigated. These will be presented in forthcoming papers. Thus the SOM approach may be a useful additional tool in guiding the development of new HEA compositions. Finally, the values in figures 10 and 11 appear to be well distributed according to the three domains identified from figures 2a, 3a and 3b. This result supports the idea that the simple rule based on the two Hume-Rothery parameters, *e/a* and *r*, is sufficient to classify HEAs according to phases in a first step.

4. Conclusions

According to a Hume-Rothery approach *e/a* and the average radius can give a very precise methodology to identify the domain of stability of HEAs, and to estimate the phases that may occur in an alloy:

i) $e/a < 1.65$: *fcc*,

ii) $1.65 < e/a < 2.05$: mixed phases including in particular *sigma*,

iii) $e/a > 2.05$: *bcc*.

According to the Hume-Rothery approach, *e/a* is to be preferred to *VEC* to classify phases in HEAs.

Furthermore the simple combination of *e/a* and *r* gives an accurate first estimation to identify compositions with simple phases giving simple diffraction patterns, thus true HEAs as opposed to other compositional domains where complex phases occur.

Self-organizing maps can be used to make predictions for new compositions of HEAs possessing suitable phases for specific properties.

Acknowledgments: MCD is thankful for the European project AccMet NMP4-LA-2011-263206 for support.

References

[1] J.W. Yeh, S.K. Chen, S.J. Lin, J.Y. Gan, T.S. Chin, T.T. Shun, C.H. Tsau, S.Y. Chang, Nanostructured high-entropy alloys with multiple principal elements: novel alloy design concepts and outcomes, Adv. Eng. Mater. 6 (2004) 299-303.
[2] B. Cantor, I.T.H. Chang, P. Knight, A.J.B. Vincent, Microstructural development in equiatomic multicomponent alloys, Mater. Sci. Eng. A 375-377 (2004) 213-218.
[3] O.N. Senkov, J.D. Miller, D.B. Miracle, C. Woodward, Accelerated exploration of multi-principal element alloys with solid solution phases, Nature Communications 6 (2015) 6529.
[4] X. Yang, Y. Zhang, Prediction of high-entropy stabilized solid-solution in multi-component alloys, Materials Chemistry and Physics, 132 (2012) 233–238.
[5] M.H. Tsai, J.W. Yeh, High-entropy alloys: A critical review, Mater. Res. Lett. 2-3 (2014) 107-123.
[6] Y. Zhang, T.T Zuo, Z. Tang, §§M.C Gao, K.A. Dahmen, P.K. Liaw, Z.P. Lu, Microstructures and properties of high-entropy alloys, Prog. Mater. Sci. 61 (2014) 1-93.
[7] D.B. Miracle, O.N. Senkov, A critical review of high entropy alloys and related concepts, Acta Materialia 122 (2017) 448–511.
[8] D.B. Miracle, J.D. Miller, O.N. Senkov, C. Woodward, M.D. Uchic, J. Tiley, Exploration and Development of High Entropy Alloys for Structural Applications, Entropy 16 (2014) 494-525.

[9] Z.P Lu, H. Wang, M.W. Chen, I. Baker, J.W. Yeh, C.T. Liu, T.G. Nieh, An assessment on the future development of high-entropy alloys: Summary from a recent workshop, Intermetallics, 66 (2015) 67-76.
[10] M.C. Gao, J.W. Yeh, P.K. Liaw, Y. Zhang Y. High-Entropy alloys: Fundamentals and applications, Springer, 2016.
[11] R. Kozak, A. Sologubenko, W. Steurer, Single-phase high-entropy alloys – an overview, Z. Kristallogr. 230 (2015) 55–68.
[12] M.C. Gao, D.E. Alman, Searching for Next Single-Phase High-Entropy Alloy Compositions, Entropy, 15 (2013) 4504-4519.
[13] F. Tian, L.K. Varga, N. Chen, J. Shen, L. Vitos, Empirical design of single phase high-entropy alloys with high hardness, Intermetallics 58 (2015) 1-6.
[14] L. Jiang, Y.P. Lu, H. Jiang, T.M. Wang, B.N. Wei, Z.Q. Cao, T.J. Li, Formation rules of single phase solid solution in high entropy alloys. Materials Science and Technology 32 (2016) 588-592.
[15] F. Otto, Y. Yang, H. Bei, E.P. George, Relative effects of enthalpy and entropy on the phase stability of equiatomic high-entropy alloys, Acta Materialia 61 (2013) 2628–2638.
[16] Y.F. Ye, Q. Wang, J. Lu, C.T. Liu, Y. Yang, Design of high entropy alloys: A single-parameter thermodynamic rule, Scripta Materialia 104 (2015) 53–55.
[17] T. Tancret, I. Toda-Caraballo, E. Menou, P.E.J. Rivera Díaz-Del-Castillo, Designing high entropy alloys employing thermodynamics and Gaussian process statistical analysis. Materials & Design (in press).
[18] F. Zhang, C. Zhang, S.L. Chen, J. Zhu, W.S. Cao, U.R. Kattner, An understanding of high entropy alloys from phase diagram calculations, CALPHAD: Computer Coupling of Phase Diagrams and Thermochemistry 45 (2014) 1–10.
[19] O.N. Senkov, D.B. Miracle, A new thermodynamic parameter to predict formation of solid solution or intermetallic phases in high entropy alloys, J. Alloys Compd. 658 (2016) 603-607.
[20] D. Ma, B. Grabowski, F. Körmann, J. Neugebauer, D. Raabe, Ab initio thermodynamics of the CoCrFeMnNi high entropy alloy: Importance of entropy contributions beyond the configurational one, Acta Materialia 100 (2015) 90–97.
[21] I. Toda-Caraballo, P.E.J. Rivera Díaz-Del-Castillo, A criterion for the formation of high entropy alloys based on lattice distortion, Intermetallics 71 (2016) 76-87.

[22] Z. Wang, W. Qiu, Y. Yang, C.T. Liu, Atomic-size and lattice-distortion effects in newly developed high-entropy alloys with multiple principal elements, Intermetallics 64 (2015) 63-69.
[23] M.C. Troparevsky, J.R. Morris, P.R.C Kent, A.R. Lupini, G. Malcolm Stocks, Criteria for Predicting the Formation of Single-Phase High-Entropy Alloys, Phys. Rev. X 5 (2015) 011041.
[24] M.G. Poletti, L. Battezzati, Electronic and thermodynamic criteria for the occurrence of high entropy alloys in metallic systems, Acta Materialia 75 (2014) 297–306.
[25] Y. Lu, Y. Dong, L. Jiang, T. Wang, T. Li, Y. Zhang, A Criterion for Topological Close-Packed Phase Formation in High Entropy Alloys, Entropy 17 (2015) 2355-2366.
[26] Z. Leong, J.S. Wróbel, S.L. Dudarev, R. Goodall, I. Todd, D. Nguyen-Manh, The Effect of Electronic Structure on the Phases Present in High Entropy Alloys, Scientific Report 7 (2017) 39803.
[27] Y.M. Zhang, J.R.G. Evans, S. Yang, The prediction of solid solubility of alloys: developments and applications of Hume-Rothery's rules, The Journal of Crystallization Physics and Chemistry 1 (2010) 103-119.
[28] S.A. Firstov, V.F. Gorban', N.A. Krapivka N.A.; M.V. Karpets, E.P. Pechkovskii, Effect of electron density on phase composition of high-entropy equiatomic alloys, Powder Metallurgy and Metal Ceramics 54 (2016) 607-613.
[29] S. Guo, C. Ng, J. Lu, C.T. Liu, Effect of valence electron concentration on stability of fcc or bcc phase in high entropy alloys, J. Applied Phys. 109 (2011) 103505.
[30] A. Cunliffe, J. Plummer, I. Figueroa, I. Todd, Glass formation in a high entropy alloy system by design. Intermetallics 23 (2012) 204-207.
[|31] C. Dong, The concept of the approximants of quasicrystals, Scripta Materialia 33 (1995) 239-243.
[32] J.B. Qiang, D.H. Wang, C.M. Bao, Y.M. Wang, W.P. Xu, M.L. Song, C. Dong, Formation rule for Al-based ternary quasi-crystals: Example of Al–Ni–Fe decagonal phase, J. Mater. Res. 16 (2001) 2653–2660.
[33] Y.M. Wang, C.H. Shek, J.B. Qiang, C.H. Wong, Q. Wang, X.F. Zhang, C. Dong, The e/a Criterion for the Largest Glass-forming Abilities of the Zr-Al-Ni(Co) Alloys, Materials Transactions 45 (2004) 1180-1183.
[34] C. Dong, W. Chen, Y. Wang, J. Qiang, Q. Wang, Y. Lei, M. Calvo-Dahlborg, J.M. Dubois, Formation of quasicrystals and metallic glasses in relation to icosahedral clusters, J. Non-Cryst. Sol. 353 (2007) 3405–3411.

[35] W.H. Wang, C. Dong, C.H. Shek, Bulk metallic glasses, Mat. Sci. Eng. R 44 (2004) 45–89.
[36] C. Dong, Y. Wang, J. Qiang, D. Wang, W. Chen, C.H. Shek, Composition Rules from Electron Concentration and Atomic Size Factors in Zr-Al-Cu-Ni Bulk Metallic Glasses, Materials Transactions 45 (2004) 1177-1179.
[37] G. Han, J. Qiang, F. Li, L. Yuan, S. Quan, Q. Wang, Y. Wang, C. Dong, P. Haussler, The e/a values of ideal metallic glasses in relation to cluster formulae, Acta Materialia 59 (2011) 5917–5923.
[38] J. Cornide, U. Dahlborg, Z. Leong, L. Asensio Dominguez, J. Juraszek, S. Jouen, T. Hansen, R. Wunderlich, S. Chambreland, I. Todd, R. Goodall, M. Calvo-Dahlborg, Structure and properties of some CoCrFeNi-based high Entropy alloys, The Minerals, Metals & Materials Society (2015) in TMS2015 Supplemental Proceedings, John Wiley & Sons, Inc., Hoboken, NJ, USA. doi: 10.1002/9781119093466.ch139.
[39] U. Dahlborg, J. Cornide, M. Calvo-Dahlborg, T. Hansen, Z. Leong, L. Asensio Dominguez, S. Chambreland, A. Cunliffe, R. Goodall, I. Todd, Crystalline structures of some High Entropy Alloys obtained by Neutron and X-ray diffraction, Acta. Phys. Polonica A 128 (2015) 552-556.
[40] J. Cornide, M. Calvo-Dahlborg, S. Chambreland, L. Asensio Dominguez, Z. Leong, U. Dahlborg, A. Cunliffe, R. Goodall, I. Todd, Acta. Phys. Polonica A 128 (2015) 557-560.
[41] U. Dahlborg, J. Cornide, M. Calvo-Dahlborg, T. Hansen, A. Fitch, Z. Leong, S. Chambreland, R. Goodall, Structure of some CoCrFeyNi and CoCrFeNiPdx multicomponent HEA alloys by diffraction techniques, J. Alloys Compd. 681 (2016) 330-341.
[42] M. Calvo-Dahlborg, J. Cornide, U. Dahlborg, S. Chambreland, G.D. Hatton, A. Fones, Structural and microstructural characterization of CoCrFeNiPd High Entropy Alloys, Solid State Phenomena 257 (2017) 72.
[43] M. Calvo-Dahlborg, J. Cornide, F. Richomme, S. Jouen, J. Juraszek, Personal communication, 2016. To be submitted.
[44] T. Kohonen, Self-Organized Formation of Topologically Correct Feature Maps. Biol. Cybern. 43 (1982) 59-69.
[45] E. Alhoniemi, J. Himberg, J. Hollmen, S. Laine, P. Lehtimaki, K. Raivio, T. Simila, O. Simula, M. Sirola, M. Sulkava, J. Tikka, J. Vesantoc, Biennial report 2002-2003. K. Puolamäki, L. Koivisto (Eds), Otaniemi, Helsinki University of Technology. Laboratory of Computer and Information Science, 2004, pp 171-177.

[46] J. Ong, S.S. Raza Abidi, Data Mining Using Self-Organizing Kohonen maps: A Technique for Effective Data Clustering & Visualisation. International Conference on Artificial Intelligence (IC-AI'99), June 28-July 1 1999, Las Vegas.
[47] O. Grygoras, Y. Zhou, Z. Jorgensen, Minimum Spanning Tree Based Clustering Algorithms. 2012 IEEE 24th International Conference on Tools with Artificial Intelligence (2006) Arlington, Virginia. Nov. 13, 2006 to Nov. 15. ISSN: 1082-3409. ISBN: 0-7695-2728-0ictai06.
[48] W. Hume-Rothery, G.W. Mabbot, Channel Evans K.M. The freezing points, melting points and solid solubility limits of the alloys of silver and copper with the elements of the B-sub-groups, Phil. Trans. Royal soc. London A 232 (1934) 1-97.
[49] W. Hume-Rothery, G.V. Raynor, The application of X-ray methods to the determination of phase-boundaries in metallurgical equilibrium diagrams, J. Sci. Instrum. 18 (1941) 74-81.
[50] W. Hume-Rothery, Atomic diameters, atomic volumes, and solid Solubility relations in alloys, Acta Metallurgica 14 (1966) 17-20.
[51] G.P. Tiwari, R.V. Ramanujan, Review The relation between the electron to atom ratio and some properties of metallic systems, J. Materials Science 36 (2001) 271–283.
[52] U. Mizutani, H. Sato, M. Inukai, E.S. Zijlstra, Theoretical Foundation for the Hume-Rothery Electron Concentration Rule for Structurally Complex Alloys, Acta Physica Polonica A 126 (2014) 531-534.
[53] A.A. Ogwu, T.J. Davies, Practical applications of the electron theory to improve physical and mechanical properties of engineering materials, J.Materials Science 29 (1994) 1623-1628.
[54] S.A. Cho, The Engel-Brewer theory and related physical properties of the Hume-Rothery's class-I metals, Acta Metallurgica 25 (1977) 1085-1091.
[55] U. Mizutani, M. Inukai, H. Sato, E.S. Zijlstra, Hume-Rothery stabilization mechanism and e/a determination in MI-type Al–Mn, Al–Re, Al–Re–Si, Al–Cu–Fe–Si and Al–Cu–Ru–Si 1/1-1/1-1/1 approximants – a proposal for a new Hume-Rothery electron concentration rule, Philosophical Magazine 92 (2012) 1691–1715.
[56] U. Mizutani, H. Sato, M. Inukai, Y. Nishino, E.S. Zijlstra, Electrons per Atom Ratio Determination and Hume-Rothery Electron Concentration Rule for P‑Based Polar Compounds Studied by FLAPW−Fourier Calculations, Inorg. Chem. 54 (2015) 930−946.
[57] U. Mizutani, M. Inukai, H. Sato, E.S. Zijlstra, Hume-Rothery stabilization mechanism and e/a determination for RT- and MI-type 1/1-1/1-1/1 approximants studied by FLAPW-Fourier analyses, Chem. Soc. Rev. 41 (2012) 6799–6820.

[58] D.G. Pettifor, R. Podloucky, The structures of binary compounds: Theory of the p-d bonded AB compounds, J. Phys. C: Solid State Phys. 19 (1986) 315-330.
[59] D.G. Pettifor, Theory of the crystal structures of transition metals, J. Phys. C: Solid State Phys. 3 (1970) 367-377.
[60] Y.M. Zhang, S. Yang, J.R.G. Evans, Revisiting Hume-Rothery's Rules with artificial neural networks, Acta Materialia 56 (2008) 1094–1105.
[61] G. Trambly de Laissardiere, D. Nguyen-Manh, D. Mayou, Electronic structure of complex spd Hume-Rothery phases in transition-metal aluminides. In The Science of Complex Alloy Phases, Massalski T.B., Turchi E.A. (Eds), TMS Publications , San Francisco, United States, 2005, pp 345-372.
[62] G. Trambly de Laissardiere, D. Nguyen-Manh, D. Mayou, Electronic structure of complex Hume-Rothery phases and quasicrystals in transition metal aluminides, Progress in Materials Science 50 (2005) 679–788.
[63] T.B. Massalski, Comments Concerning Some Features of Phase Diagrams and Phase Transformations, Materials Transactions 51 (2010) 583-596.
[64] L.M. Hoistad, S. Lee, The Hume-Rothery Electron Concentration Rules and Second Moment Scaling, J. Am. Chem. Soc. 113 (1991) 8216-8220.
[65] E.T. Teatum, K.A. Gschneidner Jr, J.T. Waber, Compilation of calculated data useful in predicting metallurgical behavior of the elements in binary alloy systems. Report 1968 LA-4003. UC-25. Metals, Ceramics and Materials. TID-4500, Los Alamos Scientific Laboratory. In Physical Metallurgy, vol. 1. R.W.Cahn, P. Haasen (Eds.) Elsevier, 1996.

Table 1. Available parameters used for the Self-Organizing Map.

Parameter	Definition of the parameter
1	y, as in $CoCrFeNiAl_x$ where y=4+x
2	average radius [65]
3	delta
4	average density
5	average atomic mass
6	e/a
7	VEC
8	average magnetic moment per atom at saturation at 5K
9	average magnetic moment per atom at saturation at 300K
10	main detected phase by diffraction
11	second main detected phase by diffraction
12	total of the detected phases by diffraction
13	average volume per atom calculated from the lattice constant of the 1st main phase
14	average volume per atom calculated from the lattice constant of the 2nd main phase
15	2P

Figures

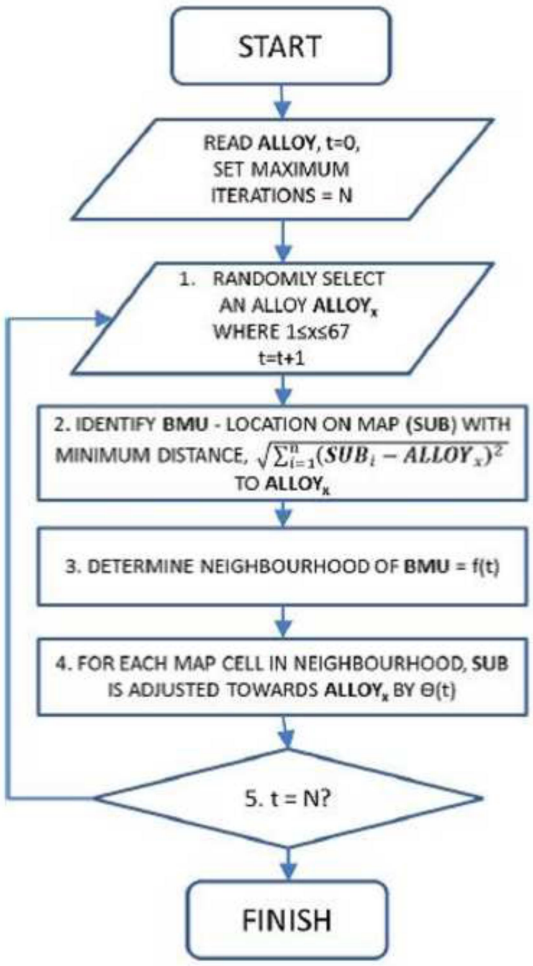

Figure 1. Flow chart of Self Organising Map algorithm.

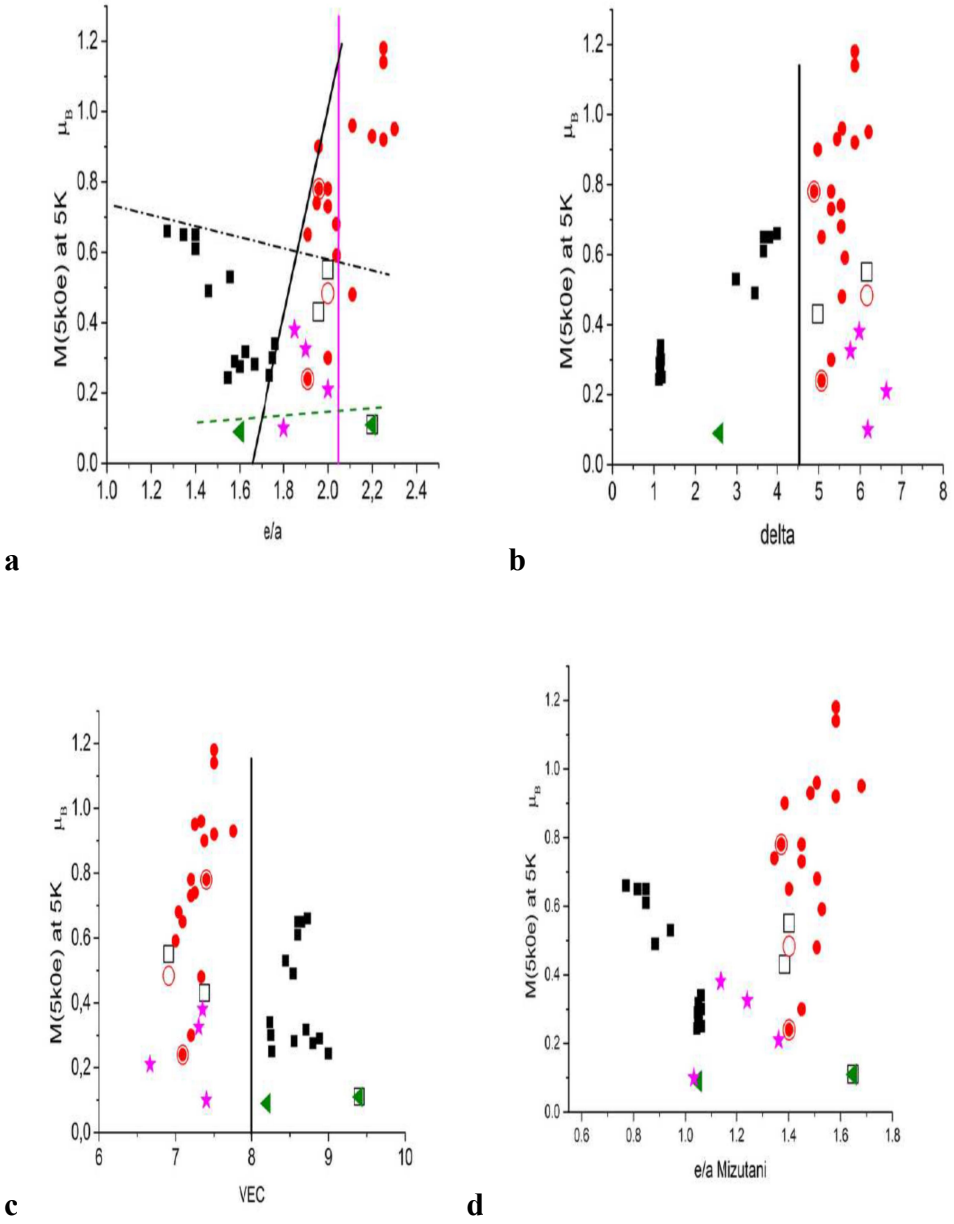

Figure 2. Variation of the experimental average magnetic moment per atom, M, at 5K [38-43] for the different detected phases (■ fcc+fcc, □ fcc+bcc, ○ bcc+fcc, ● bcc+B2, ◀ hcp, * multiple) as a function of (a) standard e/a, (b) delta and (c) VEC and (d) e/a according to Mizutani [55-57]. The bars are attempts based on visual inspection to separate phase domains.

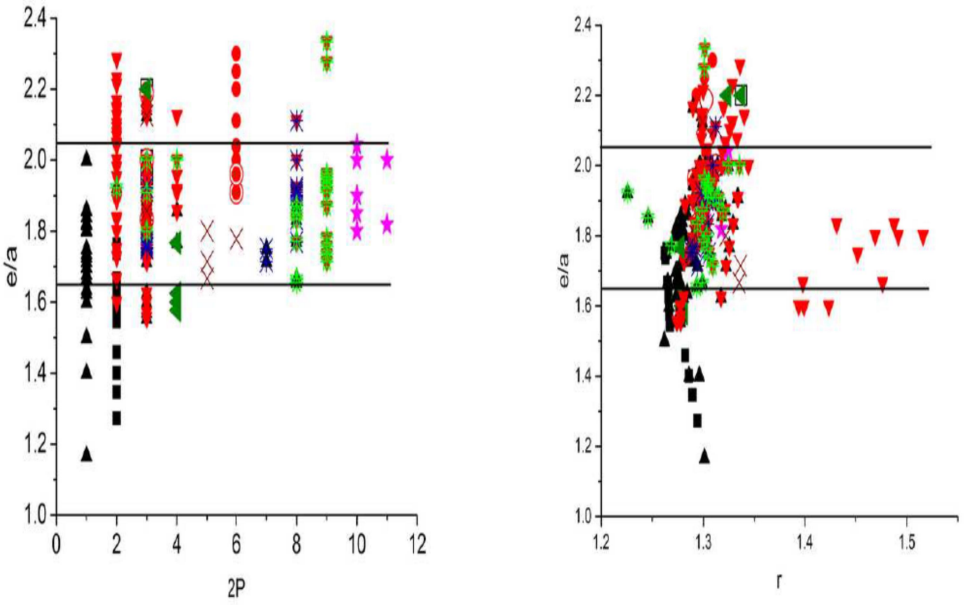

Figure 3. Variation of e/a for the different detected phases from experiments [38-43] (■ fcc+fcc, □ fcc+bcc, ○ bcc+fcc, ● bcc+B2, ◀ hcp, * multiple) and from bibliography [10,28] (▲fcc, ▼bcc, ◀hcp, *multiple, X unknown, ✳ sigma and ☆ other phases) as a function of (a) 2P, the two first main phases and (b) r, the average radius [65]. The horizontal bars are attempts based on visual inspection to separate phase domains.

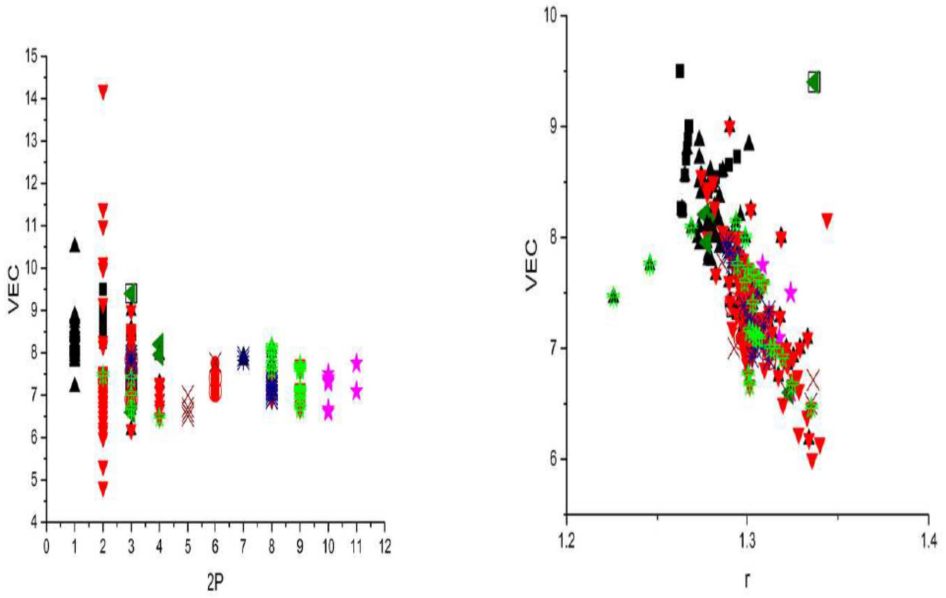

a **b**

Figure 4. Variation of VEC as a function of (a) the two first main phases and (b) the average radius [65]. For clarity the recorder detected phases are identified. From experiments [38-43] (■ fcc+fcc, □ fcc+bcc, ○ bcc+fcc, ● bcc+B2, ◀ hcp, * multiple) and from bibliography [10,28] (▲fcc, ▼bcc, ◀hcp, *multiple, X unknown, ✳ sigma and ☆ other phases).

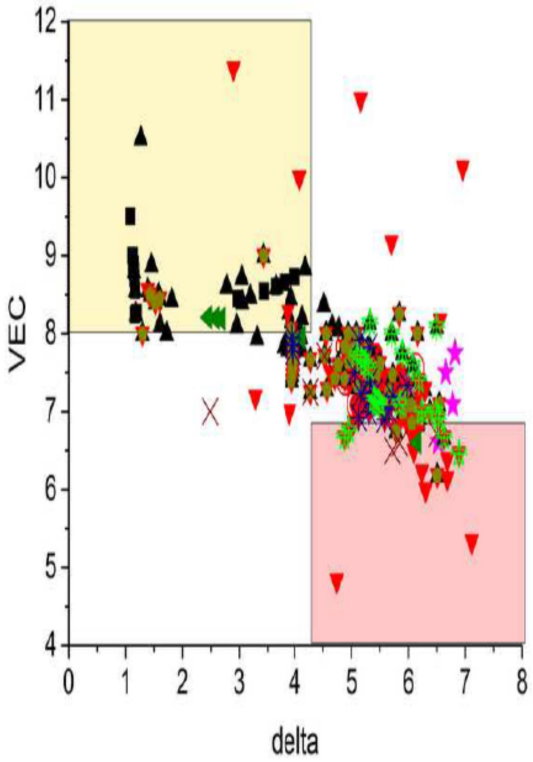

Figure 5. Variation of VEC as a function of the mismatch delta. For clarity the recorder detected phases are identified. From experiments [38-43] (■ fcc+fcc, □ fcc+bcc, ○ bcc+fcc, ● bcc+B2, ◄ hcp, * multiple) and from bibliography [10,28] (▲fcc, ▼bcc, ◄hcp, *multiple, X unknown, ✳ sigma and ☆ other phases) The coloured regions correspond to the ones identified in [14]: yellow fcc, pink .bcc.

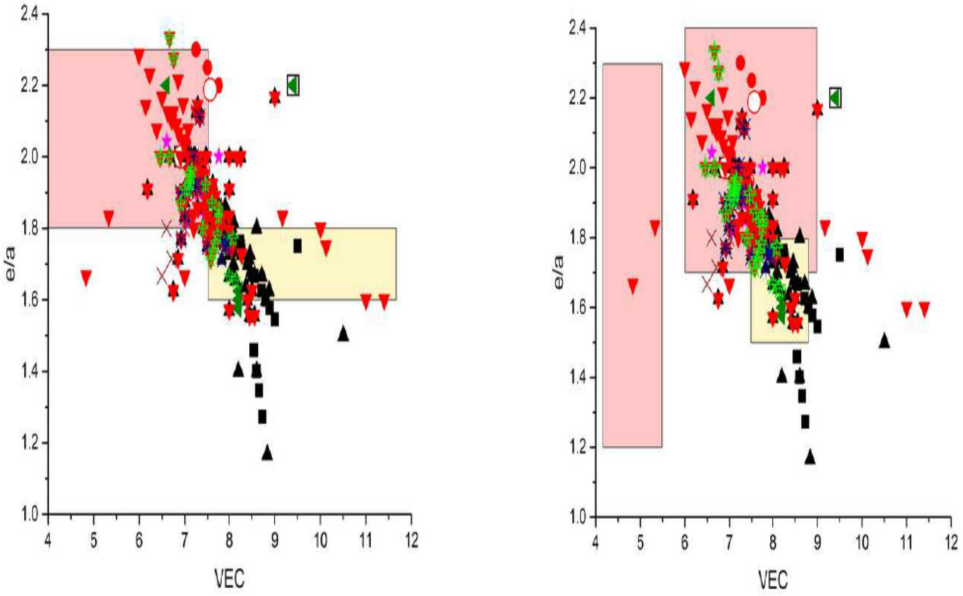

a **b**

Figure 6. Variation of e/a as a function of VEC. For clarity the recorder detected phases are identified. From experiments [38-43] (■ fcc+fcc, □ fcc+bcc, ○ bcc+fcc, ● bcc+B2, ◀ hcp, * multiple) and from bibliography [10,28] (▲fcc, ▼bcc, ◀hcp, *multiple, X unknown, ✳ sigma and ☆ other phases) The coloured regions correspond to the ones identified in (a) [24] and (b) [21]: yellow fcc, pink bcc.

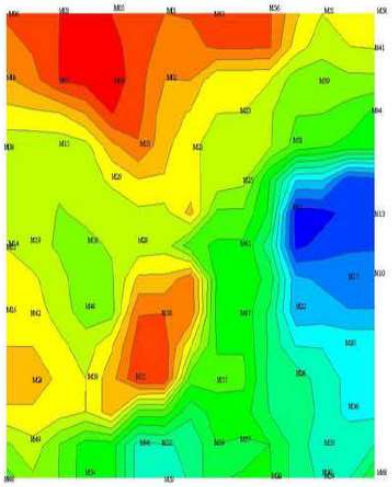

a

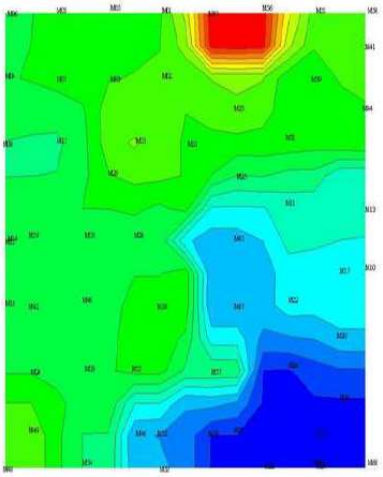

b

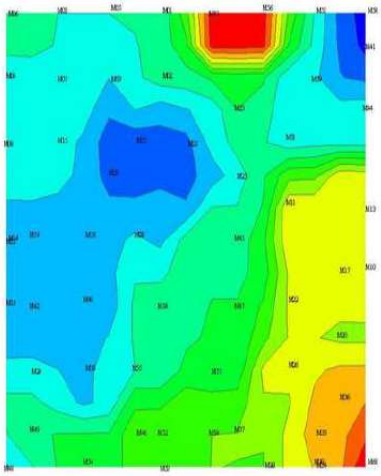

c

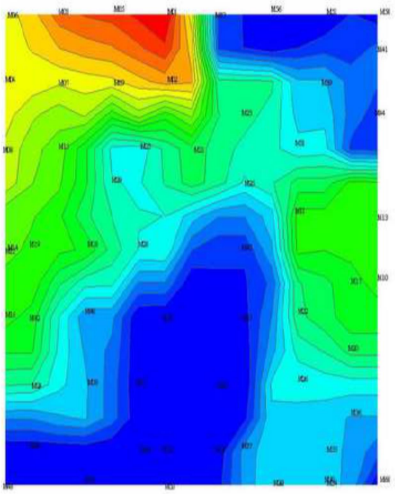

d

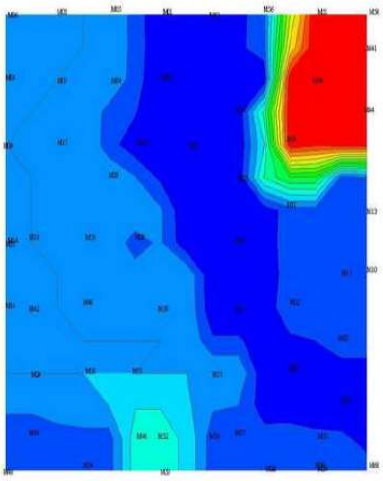

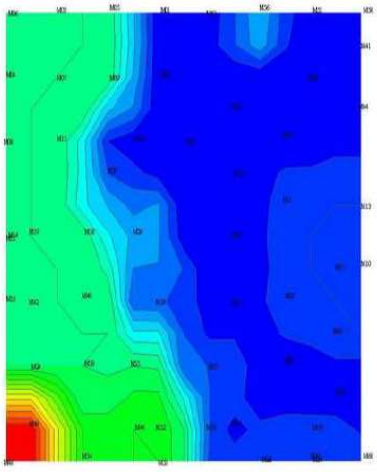

e **f**

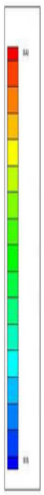

g

Figure 7. SOM results for (a) e/a, (b) delta, (c) VEC, (d) M at 5K, (e) the 1st detected phase and (f) the 2nd detected phase when **SUB** = all and all are used to construct the SOM. (g) is showing the interval of colours, red corresponding to the maximum value and blue to the minimum.

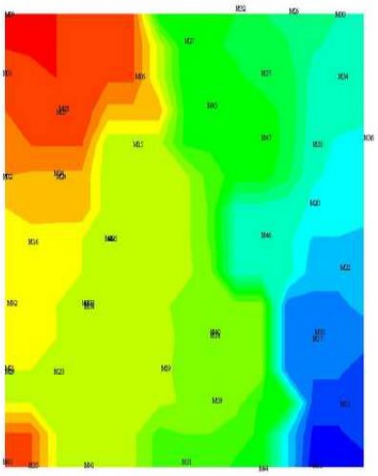

a

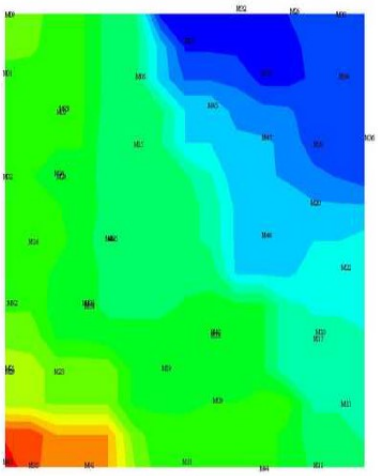

b

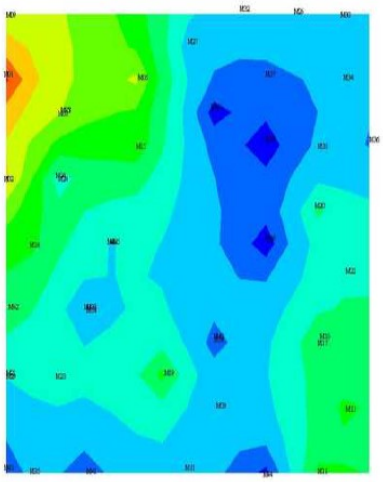

c

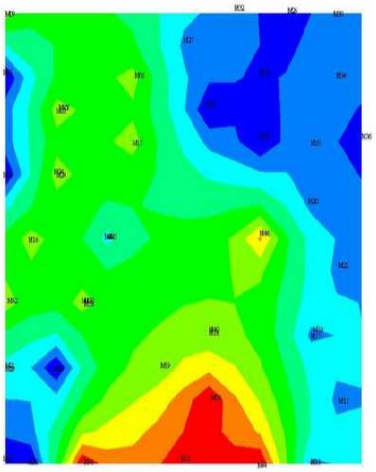

d

Figure 8. SOM results for (a) e/a, (b) r, (c) M at 5K and (d) 2P when **SUB** = e/a and r. The interval of colours, red corresponding to the maximum value and blue to the minimum, is similar as in figure 6g.

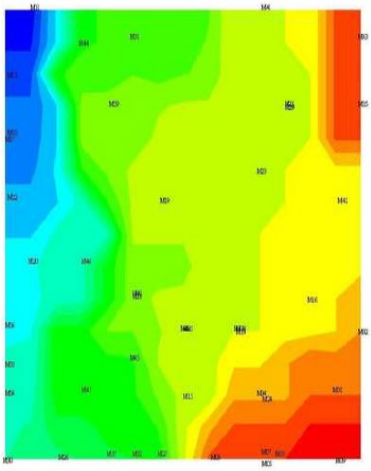

a

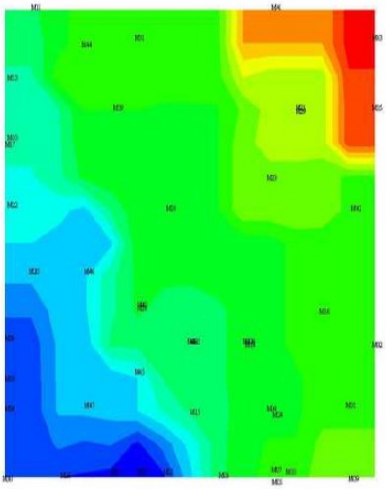

b

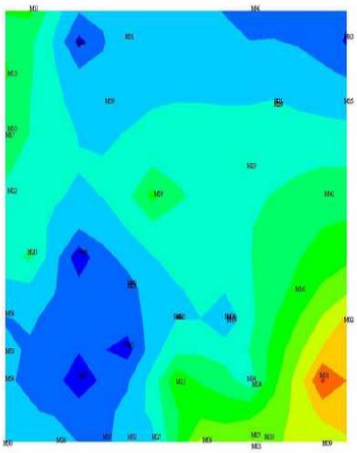

c

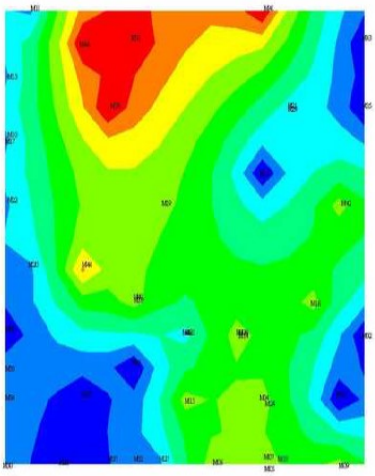

d

Figure 9. SOM results for (a) e/a, (b) r, (c) M at 5K and (d) 2P when **SUB** = e/a and r. A different random number has been chosen to start the SOM. The interval of colours, red corresponding to the maximum value and blue to the minimum, is similar as in figure 6g.

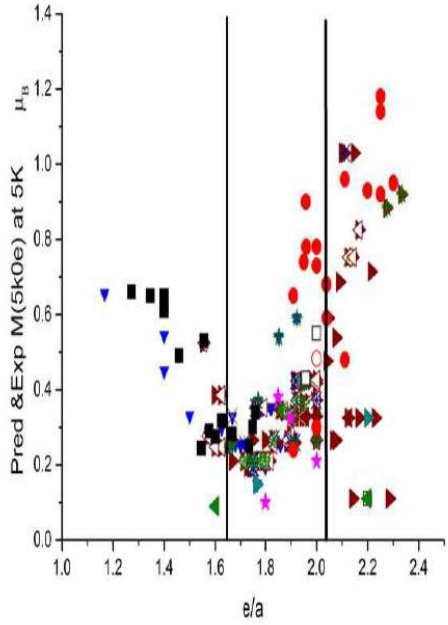

a

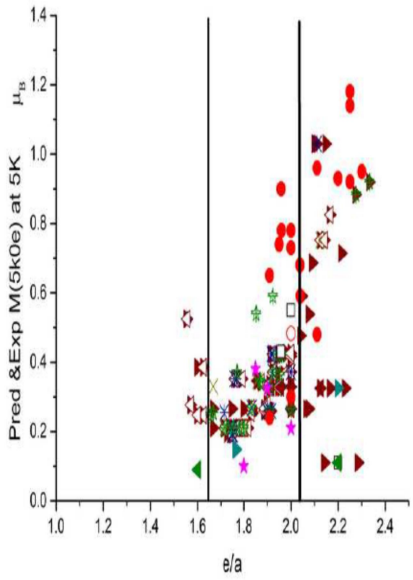

b

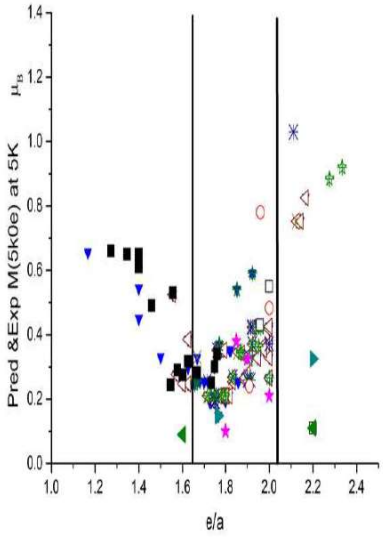

c

Figure 10. Variation of the predicted [10,28] (▼fcc, ▲fcc+fcc, Δfcc+bcc, ►bcc, □bcc+fcc, ◄bcc+bcc, □bcc+B2, ►hcp, ☆ multiple, X unknown, ✳ sigma and ✯ other phases) and experimental [38-43] (■ fcc+fcc, □ fcc+bcc, ○ bcc+fcc, ● bcc+B2, ◄ hcp, * multiple) average magnetic moment per atom at 5K as a function of e/a for (a) all alloys, (b) without alloys for which only fcc phase were identified and (c) without alloys for which only bcc phase were identified. The two vertical bars are identical to those describing the three different domains.

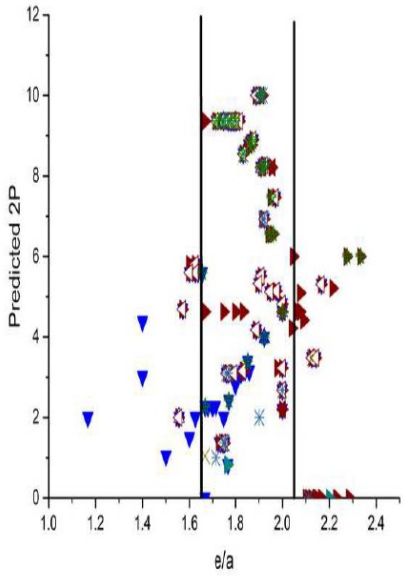

a

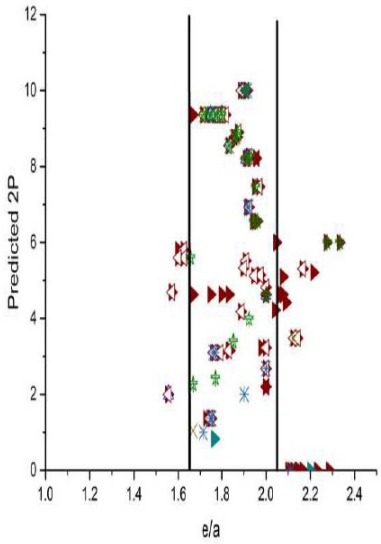

b

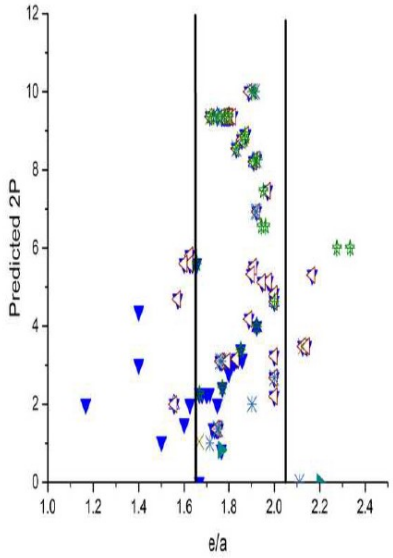

b

Figure 11. Variation of the predicted main two phases for the different alloys from bibliography [10,28] (▼fcc, ▲fcc+fcc, Δfcc+bcc, ►bcc, □bcc+fcc, ◄bcc+bcc, □bcc+B2, ►hcp, ☆multiple, X unknown, ✳ sigma and ✯ other phases) as a function of e/a. (a) all (b) without alloys for which only fcc phase were identified. (c) without alloys for which only bcc phase were identified. The two vertical bars are identical to those describing the three different domains.